An Efficient Natural Frequency-Based Method for Crack Identification in Beams

Dimitrina KINDOVA-PETROVA
Department of Technical Mechanics, University of Architecture, Civil Engineering and Geodesy, 1 Hristo Smirnenski Blvd, Sofia 1164, Bulgaria, kindova_fhe@uacg.bg

Abstract: - In recent years, frequency-based damage detection methods have attracted considerable research interest due to their cost-effectiveness, ease of implementation, and capability to detect structural damage. Such methods can be employed to localize and quantify damage by analyzing changes in natural frequencies. This paper presents a deterministic frequency-based crack identification method for beams. The crack is modeled as a massless rotational spring, and both the crack location and the associated stiffness reduction are identified through a computational procedure that exploits the analytical relationship between modal parameters and local stiffness variations. The proposed formulation employs multi-mode aggregation using the first three natural frequencies together with a modal calibration ("zero-setting") procedure, which improves robustness with respect to modeling discrepancies. To validate the proposed approach, a MATLAB-based program has been developed incorporating six different static schemes. The method is evaluated using data obtained from finite element models with various crack locations and severities. For beams with a rectangular cross-section, the program additionally enables estimation of crack depth. The results indicate that the proposed method allows accurate prediction of both crack location and severity when damage induces measurable changes in natural frequencies.

Keywords: - Crack location, Crack depth, Natural frequency, Rotational spring, Single-span beam, Optimization variables

1. INTRODUCTION

Cracks may initiate in structural elements due to fatigue, overloading, environmental effects, material imperfections, or accidental events. Since cracking is one of the main causes of structural failure, engineering structures should be regularly inspected. Various non-destructive structural health monitoring approaches have been developed to enable damage detection without compromising structural integrity. These include techniques based on ultrasonic and guided (Lamb) wave propagation, X-ray radiography, liquid penetrant inspection, infrared thermography, and optical sensing. Although these methods are effective, they are generally more labor-intensive, time-consuming, and costly when compared with vibration-based approaches.

Vibration-based methods [1–9] utilize the changes in natural frequencies and mode shapes to detect, localize, and assess the severity of structural damage. A significant number of these methods are based on the natural frequencies [10,11], as they can be easily obtained using relatively inexpensive equipment, even for inaccessible structural elements. However, natural frequency is a global characteristic of a structure and does not provide direct spatial information regarding damage location.

To overcome this limitation, various techniques have been developed to identify structural damage using frequency-related information. Zhong and Oyadiji [12,13] employed an auxiliary roving mass to obtain spatial information from frequency deviations. Çam et al. [14] excited beam vibrations by dropping a metal ball onto the structure, and analyzed the resulting response. In many studies, natural frequencies are combined with mode shapes, which are more sensitive to damage and contain local information [15,16]. Liang et al. [17] identified damage by determining the intersection point of plots relating rotational spring stiffness to crack location for three fundamental natural frequencies. Barad et al. [18] intersected curves of normalized crack location against crack depth ratio corresponding to the first and second natural frequencies. Nikolakopoulos et al. [19] constructed the contour plots describing the dependence of the first two natural frequencies on crack location and depth and identified damage by intersecting contours corresponding to the measured eigenfrequencies of the damaged beam. Springer et al. [20] determined damage location and severity from shifts in natural frequencies using the structural frequency response function. Morassi [21] applied a general perturbation approach to evaluate frequency sensitivity based on the undamaged state of the beam-like structures. Messina et al. [22] proposed a criterion using the correlation between vectors of normalized experimental natural frequency shifts and theoretical frequency shift vectors corresponding to different assumed damage locations.

Over the past two decades, numerous studies have employed stochastic optimization techniques to minimize discrepancies between measured and predicted modal responses. Talekar et al. [23] applied a fuzzy logic approach to estimate crack position and size using the first three natural frequencies obtained from experimental and theoretical analyses. Maity and Tripathy [24] employed a genetic algorithm to assess damage in a cantilever beam, defining the fitness function as the root mean square of the difference between measured and computed frequencies. Moradi et al. [25] adopted the bees algorithm to predict crack size and location in a cantilever beam by minimizing a weighted sum of squared errors between measured and computed natural frequencies. Moezi et al. [26] combined a similar objective function with the Modified Cuckoo Optimization Algorithm to identify crack location and depth, comparing the results with those obtained using the genetic Nelder-Mead algorithm and cuckoo optimization algorithm. Although these methods can provide accurate results, they rely on population-based stochastic searches and typically require numerous forward model evaluations, which increases computational cost and may affect solution repeatability.

More recently, with the rapid advancement of artificial intelligence, machine learning techniques have gained increasing attention in structural damage detection [27–30]. Their principal advantage is that they do not require explicit physics-based structural models. However, such approaches generally depend on large and representative training datasets, while data acquisition, selection, and classification processes often demand substantial computational resources and human effort. In addition, the limited physical interpretability of the identified parameters may restrict their applicability in certain engineering applications.

The proposed method offers several practical advantages. Unlike traditional approaches based on graphical solutions, which may limit accuracy and automation, the present method enables fully automatic determination of the crack parameters through a deterministic computational procedure. In contrast to metaheuristic search methods, such as genetic algorithms and the bees algorithm, which require population-based stochastic searches and numerous forward model evaluations, the proposed approach directly exploits the analytical relationship between modal parameters and local stiffness reduction. This leads to reduced computational cost and provides stable and repeatable solutions. Compared with machine-learning-based crack identification methods, the proposed approach does not require large training datasets or offline learning and retains clear physical interpretability of the identified parameters. Furthermore, relative to other frequency-based inversion techniques, the present formulation employs multi-mode aggregation using three natural frequencies together with a modal calibration ("zero-setting") procedure, which improves robustness against modeling discrepancies and reduces sensitivity to errors associated with individual modes.

The aim of the present study is to develop a method that can be incorporated into a computational program for damage localization in beams using the first three natural frequencies. For this purpose, a MATLAB-based program has been created that incorporates six different static schemes and includes crack depth prediction for beams with rectangular cross-sections. To validate the program and evaluate its accuracy, data obtained from finite element models with different damage locations and severities are used. The results indicate that even slight changes in natural frequencies enable accurate prediction of both crack location and depth in beams.

2. MODELING THE VIBRATION BEHAVIOR OF A BEAM

2.1. Undamaged beam

The governing differential equation of free transverse vibration of an Euler–Bernoulli beam is given by [18]:

$$\frac{\partial^4 w(x,t)}{\partial x^4} + \frac{\rho A}{EI}\frac{\partial^2 w(x,t)}{\partial t^2} = 0 \qquad (1)$$

where $w(x,t)$ is the transverse displacement, ρ is the mass density, A is the cross-sectional area, E is Young's modulus of elasticity, I is the area moment of inertia, t denotes time, and x is the spatial coordinate along the beam axis.

A solution of Equation (1) is sought in the form:

$$w(x,t) = W(x)\, e^{j\omega t} \qquad (2)$$

where, $j = \sqrt{-1}$ denotes the imaginary unit, ω is the natural frequency of free vibration, and $W(x)$ represents the spatial (time-independent) component of the transverse displacement. Substituting Equation (2) into Equation (1) yields:

$$\frac{d^4 W(x)}{dx^4} - \frac{\rho A \omega^2}{EI} W(x) = 0 \qquad (3)$$

Introducing the non-dimensional coordinate $\beta = x/L$, where L is the beam length, Equation (3) can be written in the following form:

$$\frac{d^4W(\beta)}{d\beta^4} - \lambda^4 W(\beta) = 0, \tag{4}$$

where λ is the non-dimensional frequency parameter, defined as:

$$\lambda^4 = \frac{\rho A L^4}{EI}\omega^2, \tag{5}$$

The general solution of Equation (4) is given by:

$$W(\beta) = C_1\cos(\lambda\beta) + C_2\sin(\lambda\beta) + C_3\cosh(\lambda\beta) + C_4\sinh(\lambda\beta), \tag{6}$$

where C_1, C_2, C_3 and C_4 are constants of integration.

Applying the boundary conditions listed in Table 1 at the beam ends yields a system of four homogeneous linear equations for the unknown constants. A non-trivial solution exists only if the determinant of the coefficient matrix is zero. Evaluating this determinant leads to the characteristic equation presented in Table 1. The roots of this equation correspond to the frequency parameters λ_i, which define the natural frequencies of the beam.

In practice, the theoretical frequency parameter of the i-th mode, $\lambda_{i,t}$, obtained from the characteristic equation, may differ from the corresponding parameter $\lambda_{i,m}$ derived from finite element simulations or experimental measurements. These discrepancies arise from modeling assumptions, material uncertainties, idealized boundary conditions, and measurement noise. To account for such differences, a modal calibration ("zero setting") procedure [30] is applied prior to damage identification, using the undamaged structure to reduce systematic discrepancies between the theoretical model and the numerical or experimental setup on a mode-by-mode basis.

For each vibration mode i, the effective modulus of elasticity $E_{i,eff}$ is adjusted so that the theoretical frequency parameter equals the measured one:

$$(\lambda_{i,t})^4 = (\lambda_{i,m})^4 = \frac{\rho A L^4}{E_{i,eff} I}\omega_{i,m}^2 \tag{7}$$

The resulting effective modulus for the i-th mode is expressed as:

$$E_{i,eff} = \frac{\rho A}{I}\omega_{i,m}^2\left(\frac{L}{\lambda_{i,t}}\right)^4, \tag{8}$$

Table 1. Boundary conditions and characteristic equations for the different beam static schemes

Static scheme	Boundary conditions	Characteristic equation
Cantilever beam 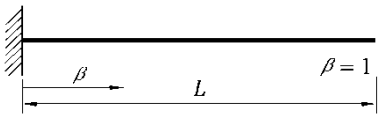	$W(0)=0,\ W'(0)=0$ $W''(1)=0,\ W'''(1)=0$	$\cos(\lambda)\cosh(\lambda)=-1$
Simply supported beam 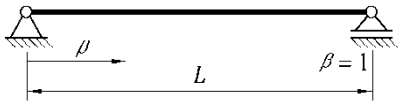	$W(0)=0,\ W''(0)=0$ $W(1)=0,\ W''(1)=0$	$\sin(\lambda)\sinh(\lambda)=0$
Fixed beam 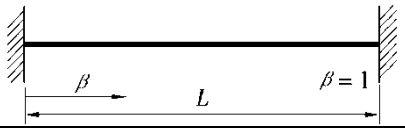	$W(0)=0,\ W'(0)=0$ $W(1)=0,\ W'(1)=0$	$\cos(\lambda)\cosh(\lambda)=1$
Propped cantilever beam 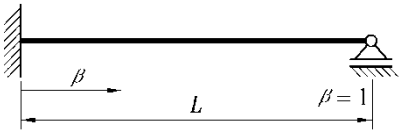	$W(0)=0,\ W'(0)=0$ $W(1)=0,\ W''(1)=0$	$\tan(\lambda)-\tanh(\lambda)=0$
Fixed-guided beam 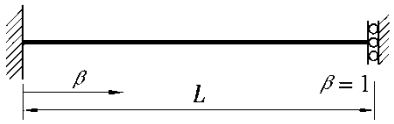	$W(0)=0,\ W'(0)=0$ $W'(1)=0,\ W'''(1)=0$	$\tan(\lambda)+\tanh(\lambda)=0$
Pinned-guided beam 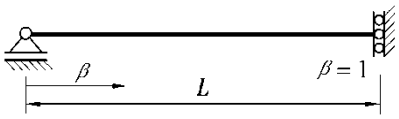	$W(0)=0,\ W''(0)=0$ $W'(1)=0,\ W'''(1)=0$	$\cos(\lambda)\cosh(\lambda)=0$

where $\omega_{i,m}$ denotes the measured natural frequency corresponding to the i-th mode.

The calibration ensures that the baseline (undamaged) model accurately reproduces the measured dynamic response before damage identification is performed. Importantly, the zero-setting procedure does not obscure the effect of damage, since the same effective modulus is

subsequently used in the inverse identification of crack location and depth. Consequently, the estimated crack depth is governed primarily by local stiffness reductions induced by the crack, while the sensitivity of the method to damage severity is maintained.

2.2. Beam with a single crack

The damage is modeled by a massless rotational spring with stiffness K_t, located at a distance L_C from the left end of the beam (see Figure 1).

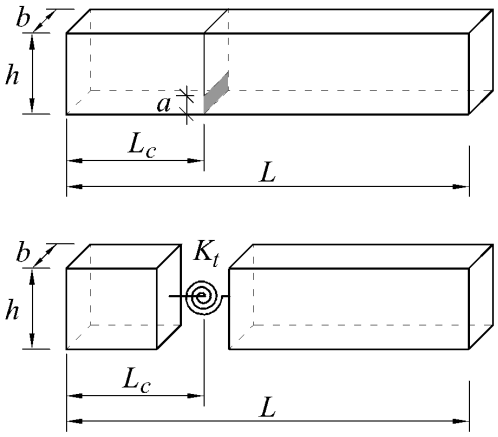

Figure 1. Representation of a crack with a rotational spring

Dimarogonas and Paipetis [32] defined the rotational constant K_t at the damage location based on the crack strain energy function for a beam with a rectangular cross-section with a single edge crack of uniform depth:

$$K_t = K\frac{EI}{L} = \frac{EI}{5.346hf_C(\alpha_C)} \tag{9}$$

where K is the non-dimensional stiffness of the rotational spring, h is the height of the beam cross-section, $\alpha_C = a/h$ denotes the normalized crack depth (see Figure 1), and $f_c(\alpha_C)$ is the dimensionless local compliance function, which has the form:

$$\begin{aligned} f_C(\alpha_C) &= 1.8624\alpha_C^2 - 3.95\alpha_C^3 + 16.375\alpha_C^4 \\ &-37.226\alpha_C^5 + 76.81\alpha_C^6 - 126.9\alpha_C^7 + 172\alpha_C^8 \\ &-143.97\alpha_C^9 + 66.56\alpha_C^{10}. \end{aligned} \tag{10}$$

The relationship between the normalized crack depth α_C and the non-dimensional stiffness K can be expressed as:

$$f_C(\alpha_C) - \frac{L}{5.346hK} = 0\,. \tag{11}$$

The governing differential equations for the two beam segments separated by the crack are:

$$\begin{aligned} &\frac{d^4W_1(\beta)}{d\beta^4} - \lambda^4 W_1(\beta) = 0,\ \ \beta\epsilon[0;\beta_c], \\ &\frac{d^4W_2(\beta)}{d\beta^4} - \lambda^4 W_2(\beta) = 0,\ \ \beta\epsilon[0;1-\beta_c], \end{aligned} \tag{12}$$

where $\beta_C = L_C / L$ is the normalized crack location.

The general solutions of Equations (12) are:

$$\begin{aligned} W_1(\beta) &= C_{1,1}\cos(\lambda\beta) + C_{1,2}\sin(\lambda\beta) + \\ &\quad C_{1,3}\cosh(\lambda\beta) + C_{1,4}\sinh(\lambda\beta), \\ W_2(\beta) &= C_{2,1}\cos(\lambda\beta) + C_{2,2}\sin(\lambda\beta) + \\ &\quad C_{2,3}\cosh(\lambda\beta) + C_{2,4}\sinh(\lambda\beta), \end{aligned} \tag{13}$$

where $C_{1,j}$ and $C_{2,j}$ (j=1, …,4) are constants of integration associated with the two beam segments.

At the crack location, continuity conditions for the displacement, bending moment, and shear force must be satisfied [33]:

$$W_1(\beta_C) = W_2(0), \tag{14}$$

$$W_1''(\beta_C) = W_2''(0), \tag{15}$$

$$W_1'''(\beta_C) = W_2'''(0), \tag{16}$$

while the matching condition for the discontinuity in the slope of the mode shape is given by [33]:

$$K\left[W_1'(\beta_C) - W_2'(0)\right] + W_1''(\beta_C) = 0 \tag{17}$$

The boundary conditions refer to the beam ends and depend on the support configuration. Applying all conditions to Equations (13) yields a system of eight linear equations, which can be written in matrix form as:

$$\mathbf{BC} = 0 \tag{18}$$

where $\mathbf{C}$ denotes the vector of the integration constants:

$$\mathbf{C} = \left[C_{1,1}\ C_{1,2}\ C_{1,3}\ C_{1,4}\ C_{2,1}\ C_{2,2}\ C_{2,3}\ C_{2,4}\right]^T \tag{19}$$

and $\mathbf{B}$ is the 8x8 coefficient matrix. The matrix $\mathbf{B}$ can be partitioned into the submatrices associated with the conditions at the beam ends ($\mathbf{B}^*$) and at the crack location

$$(\mathbf{B}^{**}):\ \mathbf{B} = \begin{bmatrix} \mathbf{B}^* \\ \mathbf{B}^{**} \end{bmatrix}. \tag{20}$$

The submatrix $\mathbf{B}^*$ depends on the beam static scheme and is given in Table 2.

The submatrix $\mathbf{B}^{**}$ is defined according to Equations (14) – (17):

$$\mathbf{B}^{**}=\begin{bmatrix} B_5 & B_6 & B_7 & B_8 & -1 & 0 & -1 & 0 \\ -B_5 & -B_6 & B_7 & B_8 & 1 & 0 & -1 & 0 \\ B_6 & -B_5 & B_8 & B_7 & 0 & 1 & 0 & -1 \\ -KB_6-B_5 & KB_5-B_6 & KB_8+B_7 & KB_7+B_8 & 0 & -K & 0 & -K \end{bmatrix}, \quad (21)$$

where $B_5 = \cos(\lambda\beta_C)$, $B_6 = \sin(\lambda\beta_C)$, $B_7 = \cosh(\lambda\beta_C)$ and $B_8 = \sinh(\lambda\beta_C)$.

For a non-trivial solution of the system, the determinant of the coefficient matrix **B** must be zero:

$$\left|\mathbf{B}\left(\lambda,\beta_c,K\right)\right|=0. \quad (22)$$

For a specified crack location β_C and rotational spring stiffness K, the roots of Equation (22) correspond to the frequency parameters λ_i.

3. CRACK LOCALIZATION AND DETERMINATION OF DAMAGE SEVERITY AS AN INVERSE PROBLEM

If a natural frequency ω_i of the damaged beam is measured, the corresponding frequency parameter λ_i may be expressed as:

$$\lambda_i = L\sqrt[4]{\frac{\rho A}{E_{i,eff}I}\omega_i^2} \quad (23)$$

Consequently, the unknown parameters in Equation (22) are the crack location β_C and the non-dimensional stiffness K. These parameters can be determined by solving the following system of nonlinear equations:

$$\begin{cases} \left|\mathbf{B}\left(\lambda_1,\beta_c,K\right)\right|=0; \\ \left|\mathbf{B}\left(\lambda_2,\beta_c,K\right)\right|=0, \end{cases} \quad (24)$$

where λ_1 and λ_2 are the frequency parameters corresponding to the first and second natural frequencies, respectively.

In the present study, the inverse problem is formulated by treating the crack location β_C and the non-dimensional stiffness K as optimization variables. Although two natural frequencies are, in principle, sufficient to identify the two unknown parameters (β_C, K), a third frequency is incorporated to improve robustness. Accordingly, the objective function is defined using the determinant of the coefficient matrix **B** evaluated for the first three natural frequencies:

$$f\left(\beta_c,K\right)=\sqrt{\sum_{i=1}^{3}\left|\mathbf{B}\left(\lambda_i,\beta_c,K\right)\right|^2} \quad (25)$$

The inclusion of an additional frequency results in an overdetermined inverse problem, which improves the numerical conditioning of the objective function by providing additional constraints and reducing sensitivity to measurement and modeling uncertainties. As a consequence, the dimensionality of the solution manifold is reduced, thereby decreasing the likelihood of multiple local minima,

Table 2. Submatrix $\mathbf{B}^*$ for the different beam static schemes

Static scheme	Submatrix $\mathbf{B}^*$
Cantilever beam	$\begin{bmatrix} 1 & 0 & 1 & 0 & 0 & 0 & 0 & 0 \\ 0 & 1 & 0 & 1 & 0 & 0 & 0 & 0 \\ 0 & 0 & 0 & 0 & B_2 & -B_1 & B_4 & B_3 \\ 0 & 0 & 0 & 0 & -B_1 & -B_2 & B_3 & B_4 \end{bmatrix}$
Simply supported beam	$\begin{bmatrix} 1 & 0 & 1 & 0 & 0 & 0 & 0 & 0 \\ -1 & 0 & 1 & 0 & 0 & 0 & 0 & 0 \\ 0 & 0 & 0 & 0 & B_1 & B_2 & B_3 & B_4 \\ 0 & 0 & 0 & 0 & -B_1 & -B_2 & B_3 & B_4 \end{bmatrix}$
Fixed beam	$\begin{bmatrix} 1 & 0 & 1 & 0 & 0 & 0 & 0 & 0 \\ 0 & 1 & 0 & 1 & 0 & 0 & 0 & 0 \\ 0 & 0 & 0 & 0 & B_1 & B_2 & B_3 & B_4 \\ 0 & 0 & 0 & 0 & -B_2 & B_1 & B_4 & B_3 \end{bmatrix}$
Propped cantilever beam	$\begin{bmatrix} 1 & 0 & 1 & 0 & 0 & 0 & 0 & 0 \\ 0 & 1 & 0 & 1 & 0 & 0 & 0 & 0 \\ 0 & 0 & 0 & 0 & B_1 & B_2 & B_3 & B_4 \\ 0 & 0 & 0 & 0 & -B_1 & -B_2 & B_3 & B_4 \end{bmatrix}$
Fixed-guided beam	$\begin{bmatrix} 1 & 0 & 1 & 0 & 0 & 0 & 0 & 0 \\ 0 & 1 & 0 & 1 & 0 & 0 & 0 & 0 \\ 0 & 0 & 0 & 0 & -B_2 & B_1 & B_4 & B_3 \\ 0 & 0 & 0 & 0 & B_2 & -B_1 & B_4 & B_3 \end{bmatrix}$
Pinned-guided beam	$\begin{bmatrix} 1 & 0 & 1 & 0 & 0 & 0 & 0 & 0 \\ -1 & 0 & 1 & 0 & 0 & 0 & 0 & 0 \\ 0 & 0 & 0 & 0 & -B_2 & B_1 & B_4 & B_3 \\ 0 & 0 & 0 & 0 & B_2 & -B_1 & B_4 & B_3 \end{bmatrix}$
$B_1=\cos(\lambda(1-\beta_C)), B_2=\sin(\lambda(1-\beta_C)),$ $B_3=\cosh(\lambda(1-\beta_C)), B_4=\sinh(\lambda(1-\beta_C))$	

although their complete elimination cannot be guaranteed, particularly when frequency shifts are very small.

The optimization variables are constrained within physically meaningful bounds to stabilize the inverse solution. The crack location β_C is restricted to $0 < \beta_C < 1$, corresponding to the normalized beam length, and further bounded as $0.04 \leq \beta_C \leq 0.96$ to avoid boundary singularities. The non-dimensional stiffness parameter K is constrained to positive values representing admissible crack severities. In the present study, K ranges from 20, corresponding to $\alpha_C \approx 0.4$, to 4000, corresponding to $\alpha_C \approx 0.03$.

To implement the proposed crack identification method, a computational program was developed in MATLAB (R2015a). The optimization problem was solved using the built-in function *fmincon* with the Sequential Quadratic Programming (SQP) algorithm. Since *fmincon* is a local optimization solver, a *MultiStart* approach was employed to explore the admissible parameter space and identify the global minimum of the objective function.

For beams with rectangular cross-sections, the program additionally computes the crack depth, which is obtained as the smallest positive real root of Equation (11), determined using MATLAB's built-in function *roots*.

4. NUMERICAL VERIFICATION

Numerical verification based on a finite element model (FEM) is performed to validate the proposed approach, providing a controlled and reliable framework in advance of future experimental investigation. To assess the accuracy of the predicted crack locations and depths, thirty-six test cases with varying crack positions and severities were analyzed for each static scheme.

The numerical analysis was carried out for beams with rectangular cross-sections containing a single crack. The natural frequencies of transverse vibrations were computed using commercial software SAP 2000 (V14). The beam was discretized by 8-node solid elements (see Figure 2), and the crack was modeled by disconnecting joints of certain solid elements.

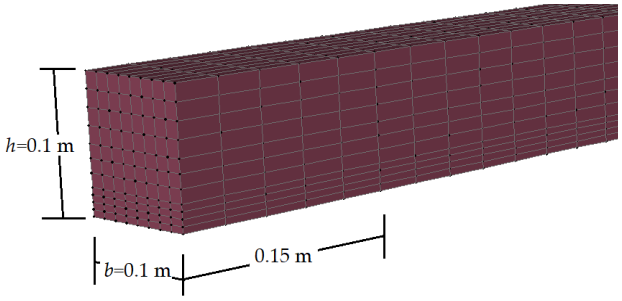

Figure 2. Part of the finite element model of the beam

The geometric and material properties of the beam are as follows: length L=3 m, height h = 0.1 m, width b = 0.1 m, Young's modulus E = 2.1 x 10^{11} N/m^2, density ρ = 7850 kg/m^3, and Poisson's ratio ν = 0.3.

Tables 3–8 present the natural frequencies obtained from the FEM analysis together with the predicted crack locations and depths. These predictions are compared with the corresponding exact reference values defined in the FEM models for the six considered static schemes. For simply supported and fixed beams, symmetrically located identical cracks produce identical changes in the natural frequencies. As a result, two symmetric crack locations represent valid solutions to the inverse problem. For this reason, Tables 4 and 5 report the results only for cracks located in the left half of the simply supported and fixed beams, respectively.

When a crack is located at a modal node, that is, at a point of zero displacement for a particular vibration mode, the presence of damage does not induce a measurable change in the natural frequency because the local stiffness reduction caused by the crack has minimal effect on the dynamic response. This behaviour can be observed at β_C = 0.5 in Table 3 (ω_3), Table 4 (ω_2), and Table 5 (ω_2); at β_C = 0.7 in Table 6 (ω_3) and Table 7 (ω_2); and at β_C = 0.4 and β_C = 0.8 in Table 8 (ω_3). This phenomenon adversely affects the accuracy of the proposed method and, in certain cases - such as case 20 of the fixed beam (Table 5) - leads to incorrect damage localization. Although the method succeeds in identifying damage in most of these cases, they should be further investigated, addressing the limitation by excluding unchanged frequencies or strategically exploiting this phenomenon for damage localization.

As can be seen in Tables 4 and 6, for the simply supported and propped cantilever beams, all predictions match the modeled crack locations and depths. Only one incorrect prediction was observed for the fixed and pinned-guided beams (Tables 5 and 8, respectively).

Four incorrect optimal solutions were obtained for the fixed-guided beam (Table 7), while the largest number of incorrect predictions (seven cases) occurred for the cantilever beam (Table 3).

These inaccuracies are primarily associated with cracks located near the free end and with cracks of normalized depth α_C = 0.05. In general, method failures occur when damage induces negligible changes in one or more natural frequencies.

Table 3. Natural frequencies from FEM and crack identification results for the cantilever beam

No	Exact normalized crack		Natural frequencies, rad/s			Predicted normalized crack		Absolute error in normalized crack	
	location $\beta_{C,e}$	depth $\alpha_{C,e}$	ω_1	ω_2	ω_3	location $\beta_{C,p}$	depth $\alpha_{C,p}$	location	depth
	undamaged		61.170	381.24	1058.4				
1	0.10	0.05	61.124	381.14	1058.3	-	-	-	-
2		0.10	60.943	380.73	1058.1	0.098	0.091	0.002	0.009
3		0.20	60.181	379.02	1057.2	0.099	0.201	0.001	0.001
4		0.30	58.892	376.24	1055.8	0.100	0.308	0	0.008
5	0.20	0.05	61.137	381.24	1058.2	-	-	-	-
6		0.10	61.009	381.23	1057.6	0.199	0.093	0.001	0.007
7		0.20	60.465	381.20	1054.8	0.200	0.203	0	0.003
8		0.30	59.532	381.15	1050.1	0.200	0.308	0	0.008
9	0.30	0.05	61.148	381.21	1057.9	-	-	-	-
10		0.10	61.063	381.05	1056.1	0.299	0.094	0.001	0.006
11		0.20	60.699	380.41	1048.7	0.300	0.201	0	0.001
12		0.30	60.068	379.30	1036.3	0.301	0.305	0.001	0.005
13	0.40	0.05	61.157	381.11	1058.1	0.388	0.042	0.012	0.008
14		0.10	61.105	380.59	1057.2	0.399	0.093	0.001	0.007
15		0.20	60.882	378.37	1053.4	0.401	0.201	0.001	0.001
16		0.30	60.491	374.59	1047.0	0.401	0.306	0.001	0.006
17	0.50	0.05	61.163	381.05	1058.4	0.497	0.040	0.003	0.010
18		0.10	61.135	380.28	1058.4	0.497	0.093	0.003	0.007
19		0.20	61.013	377.04	1058.4	0.497	0.202	0.003	0.002
20		0.30	60.799	371.53	1058.3	0.504	0.306	0.004	0.006
21	0.60	0.05	61.167	381.06	1058.1	0.601	0.041	0.001	0.009
22		0.10	61.154	380.36	1056.9	0.602	0.093	0.002	0.007
23		0.20	61.098	377.37	1052.1	0.600	0.202	0	0.002
24		0.30	60.999	372.22	1044.0	0.600	0.307	0	0.007
25	0.70	0.05	61.169	381.14	1057.8	0.705	0.040	0.005	0.010
26		0.10	61.164	380.72	1055.4	0.701	0.093	0.001	0.007
27		0.20	61.145	378.92	1045.4	0.700	0.202	0	0.002
28		0.30	61.110	375.77	1028.8	0.699	0.306	0.001	0.006
29	0.80	0.05	61.170	381.21	1058.0	0.837	0.053	0.037	0.003
30		0.10	61.169	381.07	1056.5	0.800	0.092	0	0.008
31		0.20	61.164	380.48	1049.9	0.801	0.203	0.001	0.003
32		0.30	61.157	379.42	1038.4	0.799	0.306	0.001	0.006
33	0.90	0.05	61.170	381.24	1058.3	-	-	-	-
34		0.10	61.170	381.23	1058.1	-	-	-	-
35		0.20	61.170	381.17	1057.1	-	-	-	-
36		0.30	61.169	381.07	1055.4	-	-	-	-

Table 4. Natural frequencies from FEM and crack identification results for the simply supported beam

No	Exact normalized crack		Natural frequencies, rad/s			Predicted normalized crack		Absolute error in the normalized crack	
	location $\beta_{C,e}$	depth $\alpha_{C,e}$	ω_1	ω_2	ω_3	location $\beta_{C,p}$	depth $\alpha_{C,p}$	location	depth
	undamaged		171.30	681.08	1517.4				
1	0.10	0.05	171.29	680.96	1516.9	0.103	0.040	0.003	0.010
2		0.10	171.26	680.49	1514.9	0.099	0.095	0.001	0.005
3		0.20	171.12	678.49	1506.6	0.102	0.199	0.002	0.001
4		0.30	170.87	674.94	1491.9	0.100	0.306	0	0.006
5	0.20	0.05	171.27	680.77	1516.7	0.199	0.041	0.001	0.009
6		0.10	171.15	679.56	1514.1	0.202	0.092	0.002	0.008
7		0.20	170.65	674.41	1503.0	0.201	0.201	0.001	0.001
8		0.30	169.76	665.58	1484.9	0.201	0.306	0.001	0.006
9	0.30	0.05	171.25	680.77	1517.3	0.294	0.04	0.006	0.010
10		0.10	171.02	679.56	1517.0	0.298	0.093	0.002	0.007
11		0.20	170.07	674.48	1515.9	0.301	0.202	0.001	0.002
12		0.30	168.41	665.97	1513.9	0.300	0.307	0	0.007
13	0.40	0.05	171.22	680.96	1517.1	0.403	0.042	0.003	0.008
14		0.10	170.92	680.50	1516.1	0.400	0.093	0	0.007
15		0.20	169.61	678.55	1511.8	0.400	0.201	0	0.001
16		0.30	167.35	675.24	1504.4	0.400	0.307	0	0.007
17	0.50	0.05	171.22	681.08	1516.6	0.500	0.041	0	0.009
18		0.10	170.88	681.08	1513.7	0.501	0.092	0.001	0.008
19		0.20	169.43	681.08	1501.4	0.499	0.201	0.001	0.001
20		0.30	166.95	681.07	1480.9	0.504	0.306	0.004	0.006

Table 5. Natural frequencies from FEM and crack identification results for the fixed beam

No	Exact normalized crack		Natural frequencies, rad/s			Predicted normalized crack		Absolute error in the normalized crack	
	location $\beta_{C,e}$	depth $\alpha_{C,e}$	ω_1	ω_2	ω_3	location $\beta_{C,p}$	depth $\alpha_{C,p}$	location	depth
	undamaged		387.04	1056.20	2043.4				
1	0.10	0.05	386.93	1056.10	2043.4	0.094	0.046	0.006	0.004
2		0.10	386.49	1055.90	2043.3	0.104	0.111	0.004	0.011
3		0.20	384.68	1055.10	2043.2	0.102	0.208	0.002	0.008
4		0.30	381.76	1053.70	2043.0	0.101	0.313	0.001	0.013
5	0.20	0.05	387.04	1056.00	2042.5	0.207	0.041	0.007	0.009
6		0.10	387.02	1055.40	2039.3	0.199	0.092	0.001	0.008
7		0.20	386.96	1052.60	2026.0	0.202	0.197	0.002	0.003
8		0.30	386.86	1048.00	2004.3	0.202	0.299	0.002	0.001
9	0.30	0.05	387.01	1055.70	2043.1	0.304	0.042	0.004	0.008
10		0.10	386.90	1053.90	2041.9	0.302	0.093	0.002	0.007
11		0.20	386.43	1046.50	2037.0	0.301	0.199	0.001	0.001
12		0.30	385.63	1034.20	2029.0	0.301	0.302	0.001	0.002
13	0.40	0.05	386.94	1055.90	2043.20	0.395	0.043	0.005	0.007
14		0.10	386.53	1055.00	2042.30	0.400	0.093	0	0.007
15		0.20	384.80	1051.00	2038.70	0.400	0.200	0	0
16		0.30	381.88	1044.50	2032.70	0.400	0.303	0	0.003
17	0.50	0.05	386.90	1056.20	2042.4	0.501	0.040	0.001	0.010
18		0.10	386.34	1056.20	2038.4	0.501	0.092	0.001	0.008
19		0.20	383.98	1056.20	2022.0	0.501	0.199	0.001	0.001
20		0.30	380.05	1056.20	1995.5	-	-	-	-

Table 6. Natural frequencies from FEM and crack identification results for the propped cantilever beam

No	Exact normalized crack		Natural frequencies, rad/s			Predicted normalized crack		Absolute error in the normalized crack	
	location $\beta_{C,e}$	depth $\alpha_{C,e}$	ω_1	ω_2	ω_3	location $\beta_{C,p}$	depth $\alpha_{C,p}$	location	depth
	undamaged		267.25	859.13	1771.8				
1	0.10	0.05	267.15	859.05	1771.8	0.101	0.042	0.001	0.008
2		0.10	266.76	858.75	1771.8	0.101	0.095	0.001	0.005
3		0.20	265.14	857.49	1771.8	0.101	0.207	0.001	0.007
4		0.30	262.47	855.45	1771.8	0.101	0.315	0.001	0.015
5	0.20	0.05	267.23	859.05	1771.2	0.207	0.037	0.007	0.013
6		0.10	267.18	858.76	1768.7	0.202	0.090	0.002	0.010
7		0.20	266.95	857.52	1758.0	0.201	0.199	0.001	0.001
8		0.30	266.55	855.41	1740.0	0.200	0.305	0	0.005
9	0.30	0.05	267.24	858.79	1771.4	0.307	0.040	0.007	0.010
10		0.10	267.23	857.47	1769.6	0.302	0.092	0.002	0.008
11		0.20	267.17	851.90	1762.3	0.302	0.200	0.002	0
12		0.30	267.06	842.51	1750.2	0.301	0.305	0.001	0.005
13	0.40	0.05	267.210	858.82	1771.8	0.384	0.038	0.016	0.012
14		0.10	267.040	857.61	1771.7	0.398	0.092	0.002	0.008
15		0.20	266.33	852.56	1771.2	0.401	0.201	0.001	0.001
16		0.30	265.110	844.09	1770.4	0.401	0.306	0.001	0.006
17	0.50	0.05	267.16	859.07	1771.1	0.497	0.039	0.003	0.011
18		0.10	266.79	858.85	1768.1	0.499	0.092	0.001	0.008
19		0.20	265.26	857.93	1755.7	0.500	0.201	0	0.001
20		0.30	262.65	856.36	1735.1	0.500	0.305	0	0.005
21	0.60	0.05	267.13	859.08	1771.2	0.602	0.042	0.002	0.008
22		0.10	266.67	858.91	1769.0	0.601	0.092	0.001	0.008
23		0.20	264.71	858.17	1759.6	0.601	0.200	0.001	0
24		0.30	261.36	856.93	1743.7	0.600	0.305	0	0.005
25	0.70	0.05	267.14	858.81	1771.8	0.693	0.042	0.007	0.008
26		0.10	266.73	857.57	1771.8	0.693	0.096	0.007	0.004
27		0.20	264.97	852.40	1771.7	0.699	0.202	0.001	0.002
28		0.30	261.94	843.80	1771.5	0.701	0.305	0.001	0.005
29	0.80	0.05	267.18	858.70	1771.1	0.798	0.041	0.002	0.009
30		0.10	266.94	857.06	1768.4	0.799	0.093	0.001	0.007
31		0.20	265.88	850.10	1757.3	0.799	0.201	0.001	0.001
32		0.30	264.02	838.32	1739.4	0.799	0.306	0.001	0.006
33	0.90	0.05	267.23	858.94	1771.2	0.876	0.035	0.024	0.015
34		0.10	267.16	858.23	1768.7	0.894	0.088	0.006	0.012
35		0.20	266.84	855.15	1758.0	0.897	0.196	0.003	0.004
36		0.30	266.28	849.72	1739.6	0.896	0.298	0.004	0.002

Table 7. Natural frequencies from FEM and crack identification results for the fixed-guided beam

No	Exact normalized crack		Natural frequencies, rad/s			Predicted normalized crack		Absolute error in the normalized crack	
	location $\beta_{C,e}$	depth $\alpha_{C,e}$	ω_1	ω_2	ω_3	location $\beta_{C,p}$	depth $\alpha_{C,p}$	location	depth
	undamaged		97.257	522.51	1278.0				
1	0.10	0.05	97.199	522.40	1278.0	-	-	-	-
2		0.10	96.972	521.98	1277.8	-	-	-	-
3		0.20	96.024	520.25	1277.4	0.101	0.203	0.001	0.003
4		0.30	94.465	517.47	1276.6	0.100	0.306	0	0.006
5	0.20	0.05	97.229	522.50	1277.7	-	-	-	-
6		0.10	97.117	522.50	1276.5	0.202	0.092	0.002	0.008
7		0.20	96.648	522.47	1271.6	0.201	0.199	0.001	0.001
8		0.30	95.860	522.43	1263.4	0.200	0.303	0	0.003
9	0.30	0.05	97.248	522.40	1277.4	0.298	0.042	0.002	0.008
10		0.10	97.210	522.00	1275.4	0.302	0.092	0.002	0.008
11		0.20	97.050	520.31	1266.8	0.301	0.199	0.001	0.001
12		0.30	96.778	517.45	1252.7	0.301	0.303	0.001	0.003
13	0.40	0.05	97.256	522.29	1277.9	-	-	-	-
14		0.10	97.252	521.44	1277.4	0.400	0.093	0	0.007
15		0.20	97.237	517.88	1275.6	0.401	0.201	0.001	0.001
16		0.30	97.210	511.95	1272.5	0.401	0.304	0.001	0.004
17	0.50	0.05	97.256	522.30	1277.9	0.499	0.041	0.001	0.009
18		0.10	97.252	521.51	1277.5	0.501	0.093	0.001	0.007
19		0.20	97.236	518.19	1275.8	0.501	0.201	0.001	0.001
20		0.30	97.209	512.64	1273.1	0.501	0.305	0.001	0.005
21	0.60	0.05	97.250	522.42	1277.4	0.597	0.041	0.003	0.009
22		0.10	97.221	522.10	1275.1	0.600	0.093	0	0.007
23		0.20	97.100	520.74	1265.7	0.600	0.201	0	0.001
24		0.30	96.894	518.43	1250.3	0.600	0.304	0	0.004
25	0.70	0.05	97.240	522.50	1277.5	0.673	0.037	0.027	0.013
26		0.10	97.174	522.50	1275.7	0.695	0.091	0.005	0.009
27		0.20	96.894	522.49	1268.1	0.701	0.201	0.001	0.001
28		0.30	96.420	522.46	1255.4	0.700	0.303	0	0.003
29	0.80	0.05	97.230	522.45	1278.0	0.817	0.035	0.017	0.015
30		0.10	97.126	522.23	1277.9	0.798	0.095	0.002	0.005
31		0.20	96.686	521.29	1277.7	0.801	0.201	0.001	0.001
32		0.30	95.947	519.74	1277.2	0.800	0.307	0	0.007
33	0.90	0.05	97.223	522.31	1277.7	0.906	0.040	0.006	0.010
34		0.10	97.091	521.55	1276.7	0.898	0.094	0.002	0.006
35		0.20	96.535	518.40	1272.4	0.899	0.202	0.001	0.002
36		0.30	95.603	513.28	1265.5	0.900	0.306	0	0.006

Table 8. Natural frequencies from FEM and crack identification results for the pinned-guided beam

No	Exact normalized crack		Natural frequencies, rad/s			Predicted normalized crack		Absolute error in the normalized crack	
	location $\beta_{C,e}$	depth $\alpha_{C,e}$	ω_1	ω_2	ω_3	location $\beta_{C,p}$	depth $\alpha_{C,p}$	location	depth
	undamaged		42.919	384.76	1060.6				
1	0.10	0.05	42.919	384.72	1060.3	-	-	-	-
2		0.10	42.917	384.57	1059.3	0.091	0.100	0.009	0
3		0.20	42.908	383.89	1054.8	0.100	0.201	0	0.001
4		0.30	42.892	382.68	1046.9	0.103	0.301	0.003	0.001
5	0.20	0.05	42.917	384.64	1060.0	0.172	0.044	0.028	0.006
6		0.10	42.909	384.14	1058.0	0.200	0.093	0	0.007
7		0.20	42.874	382.00	1049.3	0.201	0.201	0.001	0.001
8		0.30	42.811	378.28	1034.8	0.201	0.306	0.001	0.006
9	0.30	0.05	42.915	384.57	1060.3	0.293	0.041	0.007	0.009
10		0.10	42.897	383.83	1059.3	0.300	0.093	0	0.007
11		0.20	42.821	380.69	1055.0	0.301	0.202	0.001	0.002
12		0.30	42.687	375.31	1047.8	0.300	0.307	0	0.007
13	0.40	0.05	42.912	384.59	1060.6	0.400	0.040	0	0.010
14		0.10	42.882	383.90	1060.6	0.400	0.093	0	0.007
15		0.20	42.755	381.00	1060.6	0.400	0.202	0	0.002
16		0.30	42.532	376.07	1060.6	0.400	0.307	0	0.007
17	0.50	0.05	42.909	384.67	1060.3	0.508	0.041	0.008	0.009
18		0.10	42.866	384.29	1059.3	0.500	0.092	0	0.008
19		0.20	42.682	382.68	1054.9	0.500	0.202	0	0.002
20		0.30	42.362	379.91	1047.5	0.500	0.307	0	0.007
21	0.60	0.05	42.905	384.75	1060.0	0.621	0.044	0.021	0.006
22		0.10	42.849	384.67	1058.0	0.600	0.093	0	0.007
23		0.20	42.610	384.37	1049.3	0.601	0.201	0.001	0.001
24		0.30	42.194	383.83	1034.7	0.600	0.306	0	0.006
25	0.70	0.05	42.902	384.76	1060.3	0.681	0.038	0.019	0.012
26		0.10	42.834	384.74	1059.3	0.698	0.091	0.002	0.009
27		0.20	42.545	384.66	1054.9	0.700	0.201	0	0.001
28		0.30	42.045	384.20	1047.3	0.712	0.338	0.012	0.038
29	0.80	0.05	42.900	384.70	1060.6	0.799	0.038	0.001	0.012
30		0.10	42.822	384.43	1060.6	0.800	0.093	0	0.007
31		0.20	42.494	383.32	1060.6	0.800	0.202	0	0.002
32		0.30	41.927	381.45	1060.6	0.800	0.308	0	0.008
33	0.90	0.05	42.898	384.61	1060.3	0.915	0.039	0.015	0.011
34		0.10	42.815	384.01	1059.3	0.900	0.093	0	0.007
35		0.20	42.461	381.48	1055.0	0.900	0.202	0	0.002
36		0.30	41.852	377.29	1048.0	0.900	0.307	0	0.007

Table 9. Statistical indicators for crack location prediction

Static scheme	For crack size α_C=0.05			For crack sizes $\alpha_C \geq 0.1$		
	MaxAE	*MAE*	*RMSE*	*MaxAE*	*MAE*	*RMSE*
Cantilever beam	0.037	0.0116	0.0176	0.004	0.0010	0.0015
Simply supported beam	0.006	0.0026	0.0033	0.004	0.0011	0.0015
Fixed beam	0.007	0.0046	0.0050	0.004	0.0013	0.0016
Propped cantilever beam	0.024	0.0077	0.0105	0.007	0.0016	0.0023
Fixed-guided beam	0.027	0.0093	0.0133	0.005	0.0010	0.0014
Pinned-guided beam	0.028	0.0124	0.0155	0.012	0.0011	0.0030

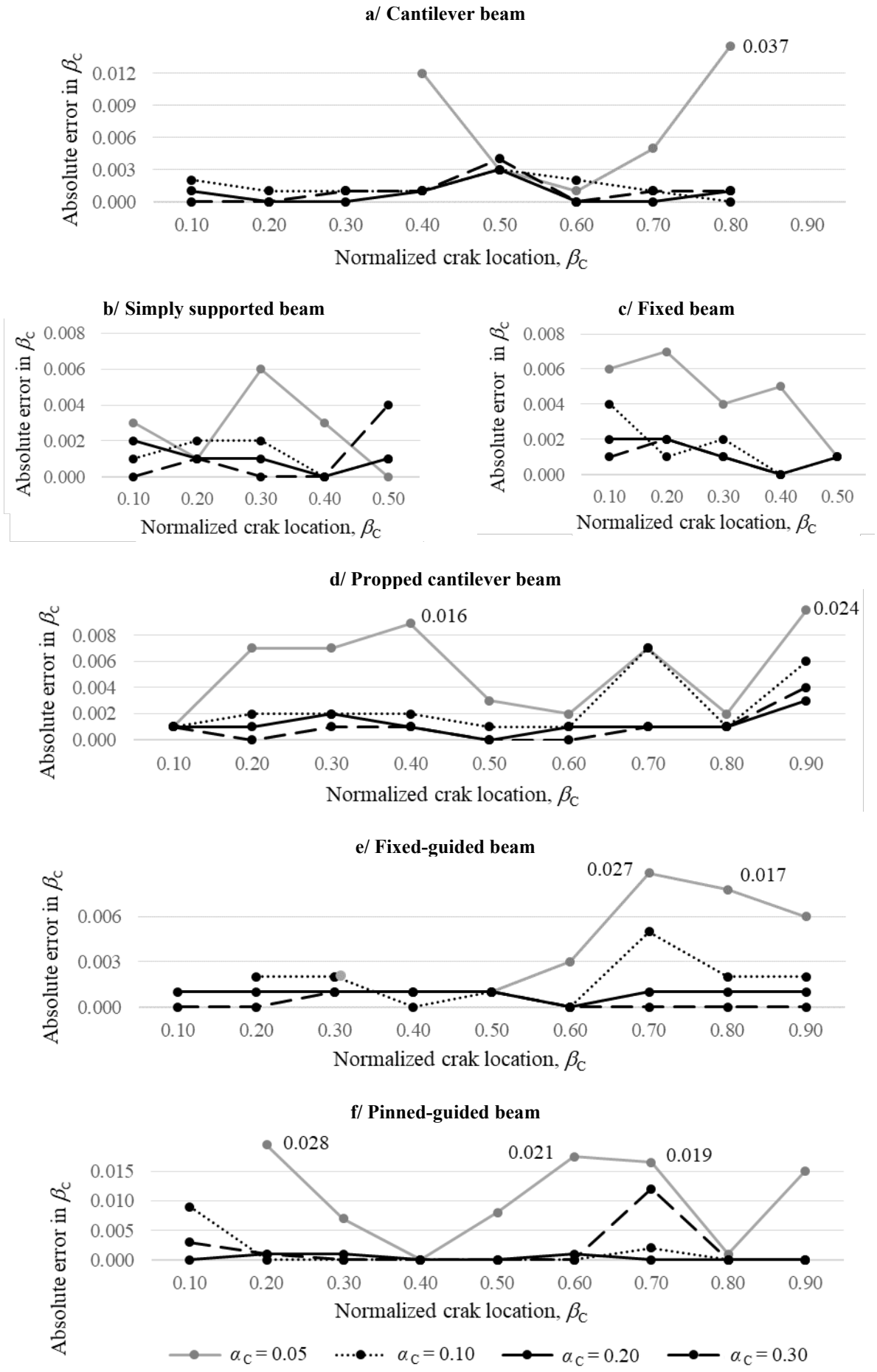

Figure 3. Absolute error in normalized crack location as a function of crack position for different crack depths

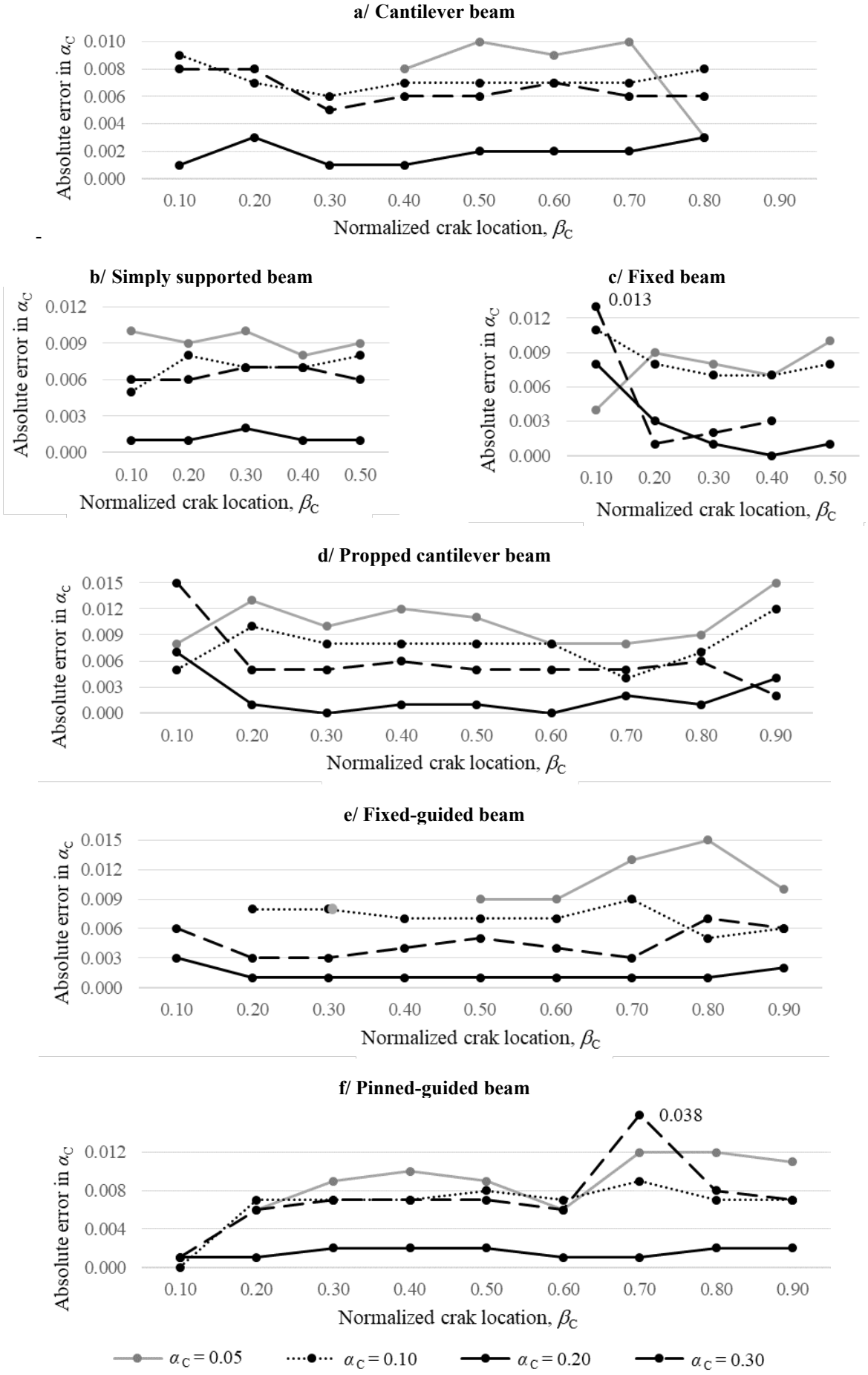

Figure 4. Absolute error in normalized crack depth as a function of crack position for different crack sizes

Table 10. Statistical indicators for crack depth prediction

Static scheme	For crack size α_C =0.05			For crack sizes $\alpha_C \geq 0.1$		
	$MaxAE_d$	MAE_d	$RMSE_d$	$MaxAE_d$ *	MAE_d	$RMSE_d$
Cantilever beam	0.010	0.0080	0.0084	0.009	0.0052	0.0058
Simply supported beam	0.010	0.0092	0.0092	0.008	0.0049	0.0053
Fixed beam	0.010	0.0076	0.0079	0.013	0.0052	0.0066
Propped cantilever beam	0.015	0.0104	0.0107	0.015	0.0052	0.0064
Fixed-guided beam	0.015	0.0107	0.0110	0.009	0.0042	0.0050
Pinned-guided beam	0.012	0.0094	0.0096	0.038	0.0059	0.0091

5. DISCUSSION

5.1. Accuracy assessment using statistical Indicators

To enhance visual interpretation, the results are also presented graphically. Figures 3 and 4 illustrate the absolute errors in crack location and crack depth, respectively, for different crack positions and sizes for the considered beam static schemes.

As can be observed from Figures 3 and 4, as well as from Tables 3 – 8, crack depths of $\alpha_C = 0.05$ are associated with larger discrepancies in both crack location and crack depth predictions compared with larger crack sizes. To access the precision of the proposed method, the following statistical indicators are employed:

$$MAE = \frac{1}{p}\sum_{k=1}^{p}\left|\beta_{C,e} - \beta_{C,p}\right|, \quad (26)$$

$$RMSE = \sqrt{\frac{1}{p}\sum_{k=1}^{p}\left(\beta_{C,e} - \beta_{C,p}\right)^2}, \quad (27)$$

where p is the number of predicted crack locations, $\beta_{C,e,}$ and $\beta_{C,p}$ denote the exact and predicted crack locations, respectively, *MAE* represents the mean absolute error, and *RMSE* denotes the root mean squared error of the predicted crack locations.

The corresponding values of *MAE*, *RMSE*, and the maximum absolute error in crack location (*MaxAE*) are presented in Table 9. As can be observed, for all beam static schemes, the error indicators significantly decrease as α_C increases from 0.05 to values greater than or equal to 0.1. This trend suggests that the proposed method achieves higher accuracy when the crack induces more pronounced variations in the natural frequencies, thereby improving damage detectability. At α_C = 0.05, the prediction errors are relatively higher, particularly for the cantilever, fixed-guided, and pinned-guided beams. Nevertheless, the average prediction error remains within acceptable limits (*RMSE* < 0.02), indicating adequate robustness of the approach even for subtle damage scenarios. For $\alpha_C \geq 0.1$, for all beam static schemes exhibit excellent agreement between the predicted and reference values, with *MAE* values around 0.001 and *RMSE* values below 0.003. These results confirm that the proposed method provides reliable crack localization and remains sensitive to damage severity across the considered beam static schemes.

The mean absolute error and the root mean squared error of the predicted crack depths are, respectively:

$$MAE_d = \frac{1}{p}\sum_{k=1}^{p}\left|\alpha_{C,e} - \alpha_{C,p}\right|, \quad (28)$$

$$RMSE_d = \sqrt{\frac{1}{p}\sum_{k=1}^{p}\left(\alpha_{C,e} - \alpha_{C,p}\right)^2}, \quad (29)$$

where $\alpha_{C,e}$ and $\alpha_{C,p}$ are the exact and predicted crack depths, respectively.

Table 10 summarizes these statistical indicators together with the maximum absolute error in crack depth ($MaxAE_d$). Similar to the trend observed for crack location, the prediction errors decrease as α_C increases from 0.05 to values greater than or equal to 0.1. However, the reduction is less pronounced for crack depth than for crack location. For all beam static schemes, at α_C = 0.05, the values of MAE_d and $RMSE_d$ are approximately 0.01. When $\alpha_C \geq 0.1$, these errors decrease by approximately a factor of two, with the exception of the pinned-guide beam, for which $RMSE_d$ remains nearly unchanged. This behavior indicates reduced sensitivity of its natural frequencies to variations in crack depth.

The highest overall performance is observed for simply supported beams. In all considered cases, the predicted crack locations and depths closely match the reference values. Even for cracks with $\alpha_C < 0.1$, where most natural frequency-based damage detection methods exhibit limited effectiveness, the

maximum absolute error in crack location does not exceed 0.006, and the maximum absolute error in crack depth remains below 0.01.

5.2. Method limitations

Although the proposed method exhibits satisfactory overall performance, several limitations should be acknowledged. Reduced identification accuracy is observed for small crack depths (α_C=0.05), where damage-induced changes in natural frequencies are weak. A similar reduction in sensitivity occurs when the crack is located near modal nodes or close to free-end regions, where the presence of damage produces minimal frequency shifts.

In the numerical verification, the accuracy of the obtained results is influenced by the mesh density employed in the FEM. To ensure consistency and minimize numerical bias, identical mesh densities should be used for the undamaged and damaged beam models.

In practical applications, measurement noise may further reduce sensitivity to small cracks and affect identification accuracy, particularly when damage-induced frequency shifts are small. The influence of noise may be partially mitigated by the "zero-setting" procedure through the use of E_{eff}. However, reliable application of this procedure requires that frequency measurements of the undamaged and damaged structures be performed under identical environmental and operational conditions, such as temperature and boundary constraints. In practice, these conditions may not always be attainable, and baseline frequency data for the undamaged structure may be unavailable. Consequently, the effects of measurement noise and experimental uncertainties remain a limitation of the present formulation and will be addressed in future studies.

In the present work, the proposed method is applied to beams with a rectangular cross-section containing a single edge crack of uniform depth, for which established relationships between crack depth and the corresponding non-dimensional rotational spring stiffness are available. In practical situations, cracks may exhibit more complex configurations, such as inclined, curved, or non-uniform geometries, may occur in beams with different cross-sections, and may involve multiple cracks. If appropriate relationships between crack geometry and equivalent rotational spring stiffness are available for other cross-sections and crack configurations, the proposed formulation may be extended to enable crack-depth estimation in such cases. Furthermore, as the method is fundamentally based on global stiffness variations manifested through shifts in natural frequencies, it remains applicable to damage localization in beams with various cross-sections and to different types of damage that induce stiffness reduction, even in the absence of explicit crack-depth relationships.

6. CONCLUSIONS

This study demonstrates the applicability of a deterministic, physics-based frequency approach for identifying crack location and severity in beam-like structures using a limited number of natural frequencies. By exploiting analytical relationships between modal parameters and local stiffness reduction, the proposed method results in stable and repeatable identification while avoiding the high computational cost and parameter tuning associated with stochastic optimization and machine-learning-based approaches.

Numerical verification using finite element data demonstrates that the method provides reliable predictions across various beam configurations, particularly for moderate to severe damage levels. The results also indicate reduced sensitivity in cases where damage induces negligible changes in natural frequencies, thereby clarifying the practical limits of frequency-based identification techniques.

Future research will focus on experimental validation to assess the practical applicability of the proposed formulation. Planned studies will begin with small-scale laboratory experiments and progress toward full-scale beam specimens under realistic loading and boundary conditions. Further extensions of the method to beams containing multiple cracks will also be investigated.

ACKNOWLEDGMENTS

This research has been carried out with the financial support of the Research, Consultancy and Design Centre at the University of Architecture, Civil Engineering and Geodesy, Sofia, Bulgaria, under contract No BN-327/25.

REFERENCES

[1] Doebling, S.; Farrar, C., Prime, M.B., A summary review of vibration-based damage identification methods, *The Shock and Vibr. Digest*, 1998, Vol. 30, No. 2, pp. 91-105.

[2] Sohn, H.; Farrar, C.R.; Hemez, F.M.; Shunk, D.D.; Stinemates, D.W.; Nadler, B.R.; Czarnecki, J.J., A review of structural health monitoring literature: 1996–2001; *The Los Alamos National Laboratory Report, 13976-MS*; Los Alamos National Laboratory, NM, USA, 2003.

[3] Sinou, J., A review of damage detection and health monitoring of mechanical systems from changes in the measurement of linear and non-linear vibrations. In *Mechanical Vibrations: Measurement, Effects and Control*; Nova Science Publishers: New York, USA, 2009, pp. 643-702.

[4] Fan, W.; Qiao, P., Vibration-based damage identification methods: A review and comparative study, *Structural Health Monitoring*, 2011, Vol. 10, No. 1, pp. 83-111.
[5] Moughty, J.; Casas, J., A state of the art review of modal-based damage detection in bridges: development, challenges, and solutions, *Appl. Sciences*, 2017, Vol. 7, No. 5, 510.
[6] Sun, X.; Ilanko, S.; Mochida, Y.; Tighe, R.C., A review on vibration-based damage detection methods for civil structures, *Vibration*, 2023, Vol. 6, No. 4, pp. 843-875.
[7] Ren, Y.; Bareille, O.; Lin, Z.; Huang, X. Review of damage detection techniques in vibration-based structural health monitoring, *International Journal of Dynamics and Control*, 2025, Vol. 13, 99.
[8] Rabi, R.; Vailati, M.; Monti, G., Effectiveness of vibration-based techniques for damage localization and lifetime prediction in structural health monitoring of bridges: A comprehensive review, *Buildings*, 2024, Vol. 14, No. 4, 1183.
[9] Yang, Y.; Zhang, Y.; Tan, X., Review on Vibration-Based Structural Health Monitoring Techniques and Technical Codes, *Symmetry*, 2021, Vol. 13, No. 11, 1998.
[10] Salawu, O.S., Detection of structural damage through changes in frequency: A review, *Engineering Structures*, 1997, Vol. 19, No. 9, pp. 718-723.
[11] Caicedo, D.; Lara-Valencia, L.A.; Brito, J., Frequency-based methods for the detection of damage in structures: A chronological review, *DYNA*, 2021, Vol. 88, pp. 203–211.
[12] Zhong, S.; Oyadiji, S.O., Analytical predictions of natural frequencies of cracked simply supported beams with a stationary roving mass, *Journal of Sound and Vibration*, 2008, Vol. 311, No. 1-2, pp. 328-352.
[13] Zhong, S.; Oyadiji, S.O., Identification of cracks in beams with auxiliary mass spatial probing by stationary wavelet transform, *Journal of Vibration and Acoustics*, 2008, Vol. 130, No. 4, 041001.
[14] Çam, E.; Orhan, S.; Lüy, M., An analysis of cracked beam structure using impact echo method, *NDT&E International*, 2005, Vol. 38, No. 5, pp. 368-373.
[15] Capecchi, D.; Ciambella, J.; Pau, A.; Vestroni, F., Damage identification in a parabolic arch by means of natural frequencies, modal shapes and curvatures, *Meccanica*, 2016, Vol. 51, pp. 2847-2859.
[16] Yang, Y.; Liang, J.; Yuan, A.; Lu, H.; Luo, K.; Shen, X.; Wan, Q., Bridge element bending stiffness damage identification based on new indirect measurement method, *China Journal of Highway Transport*, 2021, Vol. 34, No. 2, pp. 188-198.
[17] Liang, R.; Choy, F.; Hu, J., Detection of cracks in beam structures using measurements of natural frequencies, *Journal of the Franklin Institute*, 1991, Vol. 328, No. 4, pp. 505-518.
[18] Barad, K.H.; Sharma, D.S.; Vyas, V. Crack detection in cantilever beam by frequency based method, *Procedia Engineering*, 2013, Vol. 51, pp. 770-775.
[19] Nikolakopoulos, P.G.; Katsareas, D.E.; Papadopoulost, C. A., Crack identification in frame structures, *Computers & Structures*, 1997, Vol. 64, No. 1-4, pp. 389-406.
[20] Springer, W.T.; Lawrence, K.L.; Lawley, T.J., Damage assessment based on the structural frequency-response function, *Experimental Mechanics*, 1988, Vol. 28, pp. 34-37.
[21] Morassi, A., Crack-induced changes in eigenparameters of beam structures, *Journal of Engineering Mechanics*, 1993, Vol. 119, No. 9, pp. 1798-1803.
[22] Messina, A.; Jones, A.J.; Williams, E.J., Damage detection and localization using natural frequency changes. In Proceedings of the 1st International Conference on Identification in Engineering Systems, Swansea, UK, 27-29 March 1996; 1, pp. 67-76.
[23] Talekar, V.V.; Bhanuse, V.R.; Kulkarni, J. V., Vibration analysis of cracked beam using fuzzy logic technique. In Proceedings of 2016 International Conference on Automatic Control and Dynamic Optimization Techniques (ICACDOT), Pune, India, 9-10 Sept. 2016, pp. 678-682.
[24] Maity, D.; Tripathy, R.R., Damage assessment of structures from changes in natural frequencies using genetic algorithm, *Structural Engineering and Mechanics*, 2005, Vol. 19, No. 1, pp. 21-42.
[25] Moradi, S.; Razi, P.; Fatahi, L., On the application of bees algorithm to the problem of crack detection of beam-type structures, *Computers & Structures*, 2011, Vol. 89, No. 23-24, pp. 2169-2175.
[26] Moezi, S.A.; Zakeri, E.; Zare, A.; Nedaei, M., On the application of modified cuckoo optimization algorithm to the crack detection problem of cantilever Euler-Bernoulli beam, *Computers & Structures*, 2015, Vol. 157, pp. 42-50.
[27] Jarali, O.; Logesh, K.; Khalkar, V.; Hariharasakthisudhan, P., Vibration based delamination detection in fiber metal laminates composite beam, *Romanian Journal of Acoustics and Vibration*, 2023, Vol. 20, No. 1, pp. 48-58
[28] Khalkar, V.; Oak, P.; Moshi, A.; Hariharasakthisudhan, P.; Jugulkar, L.; Bane, R., Crack detection in a cantilever beam using correlation model and machine learning approach, *Romanian Journal of Acoustics and Vibration*, 2022, Vol. 19, No. 2, pp. 121-133.
[29] Tufisi, C.; Rusu, V.C.; Gillich, G.R., Locating transverse cracks in prismatic beams using random forest method and the frequency drop, *Romanian Journal of Acoustics and Vibration*, 2021, Vol. 18, No. 2, pp.119-125.
[30] Cha, Y.; Ali, R.; Lewis, J.; Büyüköztürk, O., Deep learning-based structural health monitoring, *Automation in Construction*, 2024, Vol. 161, 105328.
[31] Nandwana, B.P.; Maiti, S.K., Modelling of vibration of beam in presence of inclined edge or internal crack for its possible detection based on frequency measurements, *Engineering Fracture Mechanics*, 1997, Vol. 58, No. 3, pp. 193-205.
[32] Dimarogonas, A.D.; Paipetis, S.A., *Analytical Methods in Rotor Dynamics*; Applied Science Publishers, 1983.
[33] Rizos, P.F.; Aspragathos, N.; Dimarogonas, A.D., Identification of crack location and magnitude in a cantilever beam from the vibration modes, *Journal of Sound and Vibration*, 1990, Vol. 138, No. 3, pp. 381–388.